



## Effect of temperature-induced phase transitions on bioleaching of chalcopyrite

Ke-xin CHANG, Yan-sheng ZHANG, Jia-ming ZHANG, Teng-fei LI, Jun WANG, Wen-qing QIN

School of Minerals Processing and Bioengineering, Central South University, Changsha 410083, China

Received 24 January 2019; accepted 3 July 2019

**Abstract:** The phase transformation of chalcopyrite and the effect of its phase status on bacterial leaching were studied. Under the protection of high-purity argon, different temperatures (203, 382 and 552 °C) were applied to natural chalcopyrite to complete the phase change. In addition, the chalcopyrite was bioleached before and after the phase change. The results show that the chalcopyrite heated at 203 and 382 °C remained in the  $\alpha$  phase, whereas the chalcopyrite changed from  $\alpha$  to  $\beta$  phase at 552 °C. The leaching rates of chalcopyrite after the phase transitions at 203, 382 and 552 °C were 32.9%, 40.5% and 60.95%, respectively. Further, the crystal lattice parameters of chalcopyrite increased and lattice energy decreased, which were the fundamental reasons for the significant increase in leaching rate. Electrochemical experiments demonstrated that with increasing annealing temperature, the polarization resistance decreased and corrosion current density increased. The higher the oxidation rate was, the higher the leaching rate was.

**Key words:** lattice parameter; chalcopyrite; phase transition; bioleaching; electrochemistry

### 1 Introduction

Bioleaching technology is considered an appropriate way to recover metal from low-grade ore, as compared to conventional technologies, due to its economical and environmentally friendly advantages [1]. Chalcopyrite is one of the most abundant and extremely important copper-bearing minerals in the world, accounting for approximately 70% of copper resources [2]. Bioleaching of low-grade chalcopyrite ore has been successfully applied to industrial applications. However, the extremely slow kinetics of leaching always restricts the development of bioleaching of chalcopyrite [3].

Stoichiometric chalcopyrite ( $\text{CuFeS}_2$ ) is a covalent copper sulfide that has a tetragonal structure and is derived from the sphalerite ( $\text{ZnS}$ ) structure [4]. The  $c$ -parameter of the tetragonal unit cell of chalcopyrite is approximately equal to the length of two overlapped unit cells of sphalerite. A unit cell of tetragonal chalcopyrite consists of four Cu atoms, four Fe atoms, and eight S atoms, in which sulfur layers separate alternating metal layers form sequential alternation of copper and iron atoms [5]. The unit-cell dimensions of chalcopyrite are  $a=b=5.2890$  Å,  $c=10.4230$  Å, and  $\alpha=\beta=\gamma=90.00^\circ$  [6].

Generally, the crystal structure of chalcopyrite has three classical modifications. The  $\alpha$  phase (natural chalcopyrite) and  $\lambda$  phase ( $a=10.598$  Å,  $c=5.380$  Å) are both tetragonal, while the  $\beta$  phase ( $a=5.328$  Å) is cubic. In an inert atmosphere, as the temperature gradually increases above 400 °C, the transformation of the basic  $\alpha$ -phase chalcopyrite into the high-temperature  $\beta$  and  $\gamma$  phases occurs with the evaporation of sulfur [7]. When the temperature reaches 550 °C, the  $\alpha$  phase passes completely into a high-temperature mixed-crystal phase ( $\gamma$ ) [8]. The tetragonal  $\gamma$  phase is unstable and turns into the cubic  $\beta$ -phase. As the temperature increases above 557 °C,  $\alpha$ -phase chalcopyrite completely decomposes into  $\beta$  phase and pyrite  $\text{FeS}_2$ . It is also reported that the cubic  $\beta$  phase is stabilized at room temperature, as sulfur is scarce, and if the temperature increases above 230 °C, the  $\beta$  phase will return to the  $\gamma$  phase [5]. However,  $\gamma$ -chalcopyrite was not considered in some studies. It could be assumed that the dissolution behavior and the kinetics of chalcopyrite with different modifications were different, which could be a key to the dissolution of chalcopyrite; however, this was not well investigated.

Some researchers have focused on enhancing the recovery rate of copper from chalcopyrite ore using various methods. Low initial  $\text{Fe}^{3+}$  concentration [9],

higher temperature and moderate to extreme thermophiles [10,11], fine grinding [12], and addition of catalyst [13–15] were considered the key factors for increasing the chalcopyrite dissolution rate. On the other hand, some studies have shown that different sources of pure chalcopyrite behaved dissimilarly during bioleaching in the same environmental conditions. ZHAO et al [16] showed that the leaching rates of two chalcopyrite samples were extremely different, and the addition of pyrite and bornite significantly changed the bioleaching behavior of chalcopyrite. Furthermore, electrochemical research indicated that the chalcopyrite that dissolved faster had significantly higher conductivity and oxidation–reduction rate. DONG et al [17] suggested that different types of chalcopyrite (pyritic chalcopyrite and porphyry chalcopyrite) had different adsorption behaviors of *Acidithiobacillus ferrooxidans*, leading to the distinct copper dissolution rate. However, only a few studies so far were performed to illuminate the effect of the nature of the chalcopyrite mineral itself on bioleaching. ZHOU et al [14] proposed a schematic theory of non-phototrophic bacteria optical energy utilization mediated by semiconducting minerals. The semiconductive property of chalcopyrite is related to its crystal structure.

The characteristics of the mineral's crystal structure itself affect the chalcopyrite bioleaching rate and should be investigated for further clarification of the bacterial leaching mechanisms. Therefore, in this study, the lattice parameter and phase of chalcopyrite minerals, including natural chalcopyrite and quenched chalcopyrite heated at the desired temperature, were investigated to explain different bioleaching behaviors of chalcopyrite, to provide theoretical basis for improving bioleaching rate of chalcopyrite.

## 2 Experimental

### 2.1 Minerals and reagents

A chalcopyrite, named chalcopyrite YS, was obtained from Yushui Copper Mine of Guangdong province of China, which was used in the desired-temperature heating experiment and subsequent bioleaching. Besides chalcopyrite YS, three types of natural chalcopyrite, named chalcopyrite A, B and C, were also chosen in bioleaching for cross-referencing. The three chalcopyrite minerals were acquired from the Guizhou, Guangxi, and Hubei provinces of China, respectively. Chemical element and X-ray diffraction (XRD) analyses showed that the four chalcopyrite minerals were all of extremely high purity. Chalcopyrite YS contained 31.2 wt.% Cu, 26.7 wt.% Fe, and 31.9 wt.% S; chalcopyrite A contained 33.32 wt.% Cu, 30.85 wt.% Fe, and 32.87 wt.% S; chalcopyrite B

contained 33.09 wt.% Cu, 31.11 wt.% Fe, and 33.74 wt.% S; and chalcopyrite C contained 32.97 wt.% Cu, 30.51 wt.% Fe, and 31.61 wt.% S. Massive chalcopyrite YS was used in the desired-temperature heating process and the chalcopyrite specimens used in bioleaching were all ground and artificially sieved to <0.074 mm. The mean particle sizes of chalcopyrite A, B, and C were 35.94, 35.75, and 30.91  $\mu\text{m}$ , respectively. All chemicals used in the work were of analytical grade.

### 2.2 Heating experiment

The heating experiment of chalcopyrite YS was conducted in an electrically heated horizontal tube furnace. The massive chalcopyrite samples (5 g) were cleaned by acetone and deposited in the ceramic groove in the heating zone of the furnace tube. The air was purged using argon and the oil vacuum bump to ensure that there was no oxygen in the tube. The setting temperatures were 203, 382, and 552 °C at a constant heating rate of 20 °C/min, and were maintained for 5 h. Upon completion of the roasting, the sample groove was moved under argon protection to the cooling zone for quenching in cold water. The quenched chalcopyrite was immediately transferred to a vial filled with nitrogen. The resulting specimens were named chalcopyrite a, b and c according to the testing temperatures from low to high, respectively, and all specimens were ground under the protection of nitrogen.

### 2.3 Determination of lattice parameter

To measure the lattice parameter of chalcopyrite, XRD was performed at room temperature using an X-ray diffractometer (Model D/Max 2500PC) with Cu  $K_{\alpha}$  radiation ( $\lambda=1.54056 \text{ \AA}$ ) and the standard Si powder was added into mineral samples at a mass fraction of 15% to ensure that the lattice parameter can be calculated accurately. The scanning angle  $2\theta$  was in the range from 20° to 60°, the step size was 0.01°, and the step time was 1 s.

### 2.4 Microorganism and growth conditions

A mixed culture containing *Acidithiobacillus ferrooxidans*, *Acidithiobacillus thiooxidans*, *Leptospirillum ferrooxidans*, *Leptospirillum ferriphilum*, and *Acidithiobacillus caldus* was used for the bioleaching of the heated chalcopyrite at 30 °C. Another mixed culture of moderately thermophilic bacteria was used in the bioleaching of three natural chalcopyrite samples at 45 °C, which contained *Leptospirillum ferriphilum*, *Sulfobacillus thermosulfidooxidans*, and *Acidithiobacillus caldus*. In the bioleaching experiment, 9K medium was used with the following composition:  $(\text{NH}_4)_2\text{SO}_4$  3.0 g/L,  $\text{K}_2\text{HPO}_4$  0.5 g/L,  $\text{MgSO}_4 \cdot 7\text{H}_2\text{O}$  0.5 g/L, KCl 0.1 g/L and  $\text{Ca}(\text{NO}_3)_2$  0.01 g/L. The mixed

cultures were incubated in 250 mL Erlenmeyer flasks in a temperature-controlled rotary shaker with a settled speed of 170 r/min. The cultures were cultivated by chalcopyrite as the sole energy source so that the bacteria could progressively adapt to the leaching environment lacking a quick energy substrate such as  $\text{Fe}^{2+}$  or S. The resulting culture would be inoculated in the Erlenmeyer flask for the bioleaching experiments. All bacteria used in the experiment were obtained from the Key Lab of Biohydrometallurgy of Ministry of Education, Central South University, Changsha, China.

### 2.5 Bioleaching experiment

Bioleaching of chalcopyrite YS, a, b, and c and chalcopyrite A, B, and C was carried out in Erlenmeyer flasks (250 mL) incubated in an orbital shaker at 170 r/min. A total of 2 g of dry chalcopyrite powder was added into the solution mixed with 95 mL of iron-free 9K medium and 5 mL of pre-adapted inoculum. The initial pH was adjusted to 1.7 by sulfuric acid at the beginning of bioleaching. The volume loss of liquor due to evaporation was supplemented by distilled water periodically, and isometric 9K medium was added to replace the aliquots taken for analysis during bioleaching. An inductively coupled plasma-atomic emission spectrometer (ICP-AES) was utilized to determine the concentration of cupric ions.

### 2.6 Electrochemical experiment

The electrochemical assay of chalcopyrite electrode was performed in a thermostatic jacketed cell with a conventional three-electrode system: working electrode of massive chalcopyrite, reference electrode (Ag/AgCl), and graphite counter electrode. The composition of electrolyte solution consisted of 9K medium without ferrous ions at pH 1.7. Nitrogen was bubbled from solution to eliminate oxygen and keep the electrochemical system stabilized. All chalcopyrite samples were cut into approximately  $d13 \text{ mm} \times 4 \text{ mm}$  cylinders with an effective surface of approximately  $1 \text{ cm}^2$ . Before each electrochemical test, the electrode surface was polished with silicon carbide paper (3000 grit) to keep the working face clean and fresh.

Cyclic voltammetry analyses were performed at a scan rate of 20 mV/s from open-circuit potential (OCP) to 800 mV (positive-going potential scan), then to -800 mV (negative-going potential scan), and back to the initial potential (positive-going potential scan). When the working electrode was immersed in electrolyte and the potential was stabilized, Tafel curves were performed at a sweep rate of 0.5 mV/s. All redox potential values were expressed against the Ag/AgCl reference electrode (3.0 mol/L KCl).

## 3 Results and discussion

### 3.1 Lattice parameter of heated chalcopyrite

Table 1 gives the values of lattice parameter of chalcopyrite specimens before and after heating at different temperatures. The lattice parameter of chalcopyrite (YS) was  $a=b=5.2894 \text{ \AA}$  and  $c=10.4221 \text{ \AA}$ . The lattices of chalcopyrite a and b, which were heated at 203 and 382 °C, respectively, were extremely similar with those of the natural chalcopyrite YS. Heating at a high temperature of 552 °C for 5 h increased the lattice parameters of chalcopyrite, of which parameter  $a$  was increased by  $0.0127 \text{ \AA}$  while parameter  $c$  was increased by  $0.0878 \text{ \AA}$ .

**Table 1** Lattice parameters of quenched chalcopyrite heated at desired temperatures

Chalcopyrite	$(a=b)/\text{\AA}$	$c/\text{\AA}$
YS (raw)	5.2894	10.4221
a (203 °C)	5.2891	10.4214
b (382 °C)	5.2895	10.4222
c (552 °C)	5.3021	10.5099

MACLEAN et al [18] reported that at 550 °C chalcopyrite was decomposed into intermediate solid solution, pyrite, and sulfur vapor. When heated chalcopyrite was quenched, the sulfur did not have enough time to transfer to the inner part of the solid solution, leading to the formation of sulfur-deficient chalcopyrite expressed by the formula  $\text{CuFeS}_{2-x}$  [19]. SHIMA [20] assumed that there was a transformation of tetragonal  $\alpha$ -phase chalcopyrite into cubic  $\beta$ -phase chalcopyrite, which has an approximate chemical composition of  $\text{CuFeS}_{1.8}$ .

In most studies [5,7,8,18–20], researchers used chalcopyrite powders or sheets to investigate the phase transformation of chalcopyrite at 550 °C. Nevertheless, in this work, we hope to keep the stoichiometric ratio as stable as possible; hence, 5 g massive chalcopyrite was used in heating process and quenched by water at the end of the process. When chalcopyrite sample was heated at 552 °C,  $\beta$ -phase chalcopyrite was generated along with the sulfur evaporation. However, an excessive volume of massive chalcopyrite impeded deeper sulfur escaping to the external environment. As a result, quenched chalcopyrite c consisted of  $\alpha$  phase and  $\beta$  phase, which can be proven by X-ray diffraction pattern (Fig. 1). As shown in Fig. 1, (204) and (033) diffraction peaks of chalcopyrite c decreased, indicating that a part of chalcopyrite turned into cubic  $\beta$  phase because these two peaks do not appear on the pattern of the cubic lattice. Through comparing the change in parameter  $a$  ( $0.0127 \text{ \AA}$ ) and  $c$  ( $0.0878 \text{ \AA}$ ), it can be noted that parameters  $a$  and  $c$

of quenched chalcopyrite  $c$  ( $a=5.302 \text{ \AA}$ ,  $c=10.5099 \text{ \AA}$ ) verged on the scale of 1:2, like two overlapped unit cells of sphalerite ( $\text{ZnS}$ ), which has been demonstrated by SHIMA [20]. The formation of  $\beta$ -phase chalcopyrite can

also be proven by the oxidation of chalcopyrite. After 2 h exposure to air, the surface of chalcopyrite  $c$  was ultramarine blue, whereas the others were yellowish, as shown in Fig. 2.

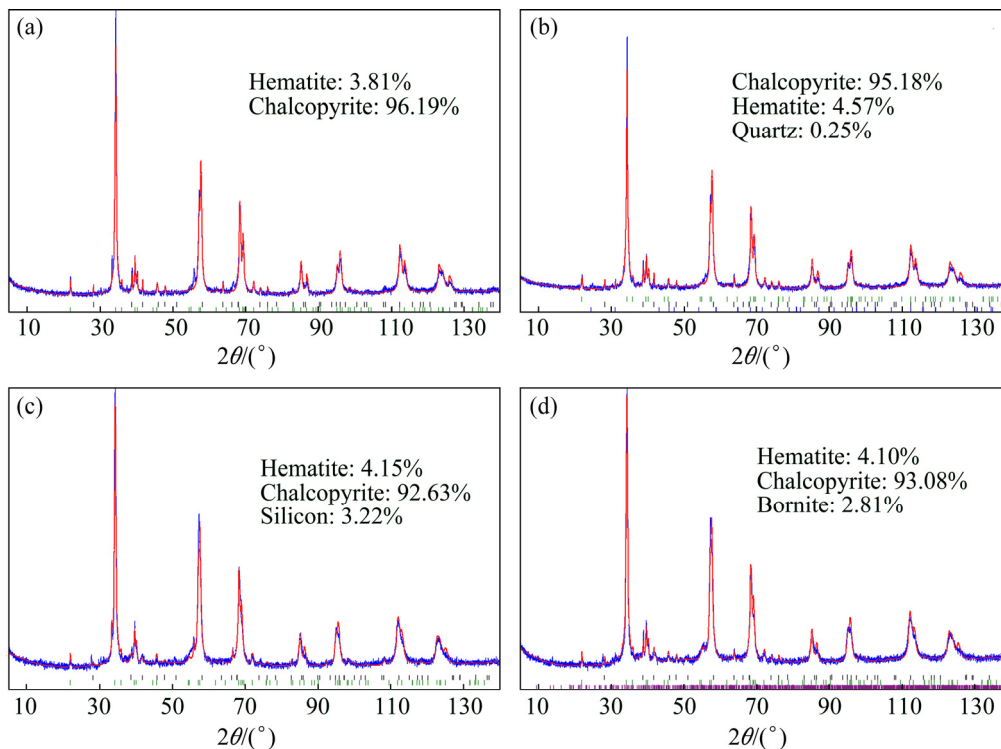


**Fig. 1** XRD patterns of chalcopyrite before and after heating: (a) Natural chalcopyrite; (b) 203 °C; (c) 382 °C; (d) 552 °C

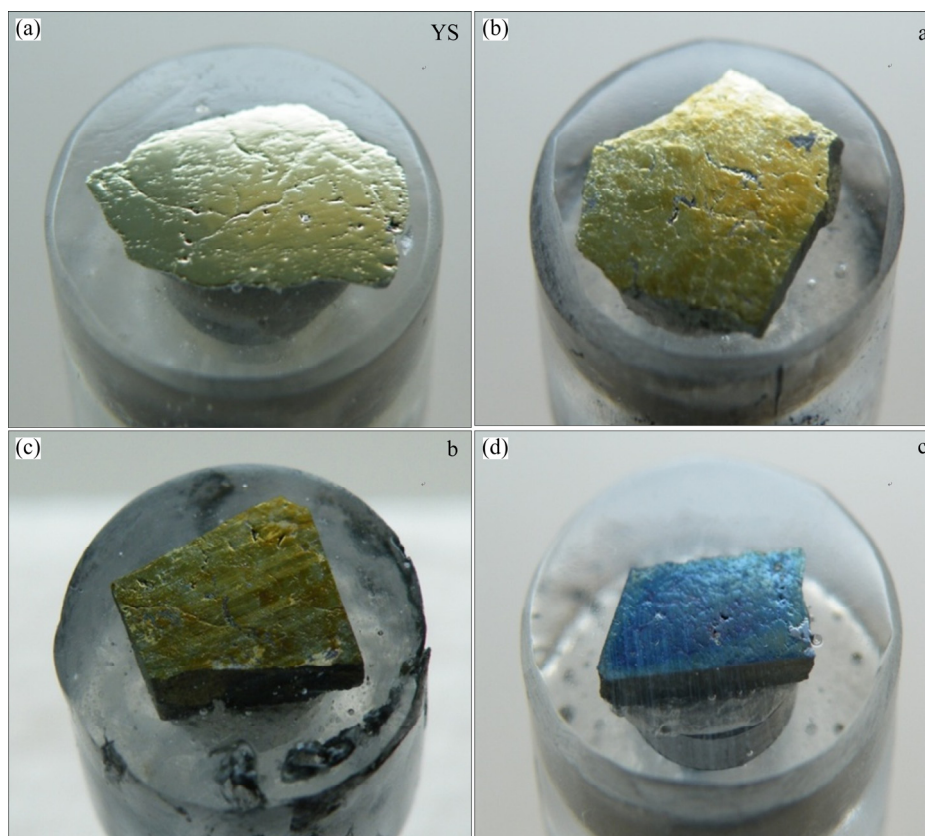


**Fig. 2** Surface appearances of natural chalcopyrite and quenched specimens after exposed to air for 2 h: (a) Raw chalcopyrite; (b) 203 °C; (c) 382 °C; (d) 552 °C

The conclusion can be drawn that at 552 °C, a part of massive chalcopyrite samples ( $\alpha$  phase) transformed to  $\beta$  phase; thus, quenched chalcopyrite c consisted of an uncertain proportion of two types of phases ( $\alpha$  and  $\beta$ ), which led to an increase in the lattice parameter. However, at 203 and 382 °C, the phase of chalcopyrite cannot be changed, resulting in no change in the lattice parameter.

### 3.2 Bioleaching of heated chalcopyrite

Figure 3 shows that four chalcopyrite specimens had variant copper recovery of bioleaching. After 23 d of bioleaching at 30 °C, the copper extractions of chalcopyrite YS, a, b and c were 31.9%, 32.9%, 40.5%, and 60.9%, respectively. The copper extraction rate of chalcopyrite c increased by 30% from the initial chalcopyrite YS, whereas that of chalcopyrite b only increased by 9.6%.

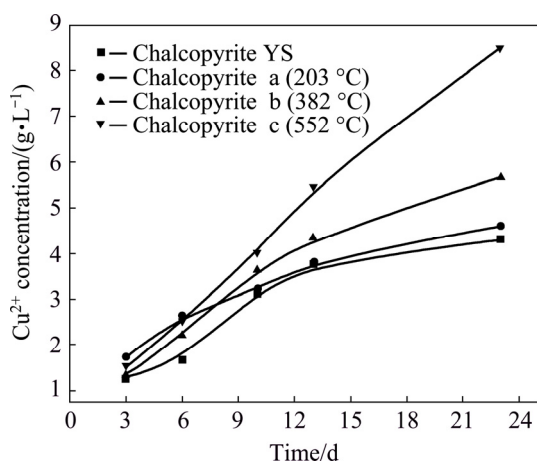


Fig. 3 Copper extraction of chalcopyrite YS and three types of heated chalcopyrite

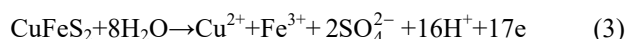
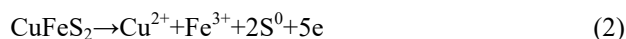
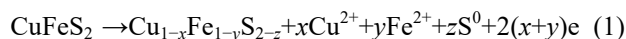
From analyzing the bioleaching results, it can be found that copper recovery rate of chalcopyrite after heating at 382 or 552 °C distinctly increases, especially at 552 °C. A greater extent of copper extraction of chalcopyrite c compared to the other three chalcopyrite specimens corresponded to the results of the lattice parameter measurement. With the transition of  $\alpha$  phase to  $\beta$  phase, chalcopyrite c heated at 552 °C had a greater degree of dissolution. It can be inferred that  $\alpha$ - $\beta$  mixed-phase chalcopyrite has a better leachability than  $\alpha$ -phase chalcopyrite, and the difference is supposed to be caused by the  $\beta$  phase. When the sample was heated at 382 °C, the copper extraction of chalcopyrite was also increased by approximately 9.6% with no formation of the  $\beta$  phase. A possible explanation for this may be that some unknown changes, rather than the lattice parameter, of the chalcopyrite mineral properties after roasting enhanced the final dissolution rate of chalcopyrite b. Further study of the changes in mineral properties after

heating at a specific temperature below the phase-transition temperature, such as 382 °C, and the resulting changes in bioleaching behavior can be supplemented.

As discussed above, when being heated at different temperatures, chalcopyrite exhibited extremely different leaching rates. Thus, electrochemical measurements were carried out to further investigate the different dissolution mechanisms of the four chalcopyrite specimens.

### 3.3 Electrochemical measurements of chalcopyrite YS and three heated chalcopyrite samples

The corresponding relationships between voltage and current of chalcopyrite YS and three heated chalcopyrite specimens during a cyclic voltammetry test in 9K electrolyte solution in the absence of ferrous ions are depicted in Fig. 4. Three anodic peaks (a1, a2, and a3) and six cathodic peaks (c1, c2, c3, c4, c5, and c6) found on the curves can be assigned to the relevant oxidation–reduction reactions reported in some studies [21–24]. When potential positively scanned from OCP to approximately 400–500 mV, chalcopyrite began to dissolve (Peak a1). Peak a1 indicates that metal ions partially dissolve from the chalcopyrite lattice, leading to the formation of metal-deficient sulfide, as shown in Eq. (1). Peak a2 is mainly considered as the oxidation of chalcopyrite into  $\text{Cu}^{2+}$  and  $\text{Fe}^{3+}$ , as shown in Eqs. (2) and (3):



In the negative scan, there are a series of cathodic peaks between 200 mV and –200 mV. Peaks c1, c2, and c3 are reductions of the oxidation products, such as copper ions and ferric ions, produced during the anodic sweep, as shown in Eqs. (4–6):



Cathodic Peak c4 was observed from approximately –100 to –300 mV, representing multiple reductions of chalcopyrite to intermediate copper sulfides, such as bornite ( $\text{Cu}_5\text{FeS}_4$ ), chalcocite ( $\text{Cu}_2\text{S}$ ), and talnakhite ( $\text{Cu}_9\text{Fe}_8\text{S}_{16}$ ), as shown in Eqs. (7–10):



In the potential range from –300 to –500 mV, Peak c5 was widely attributed to the reduction of bornite or

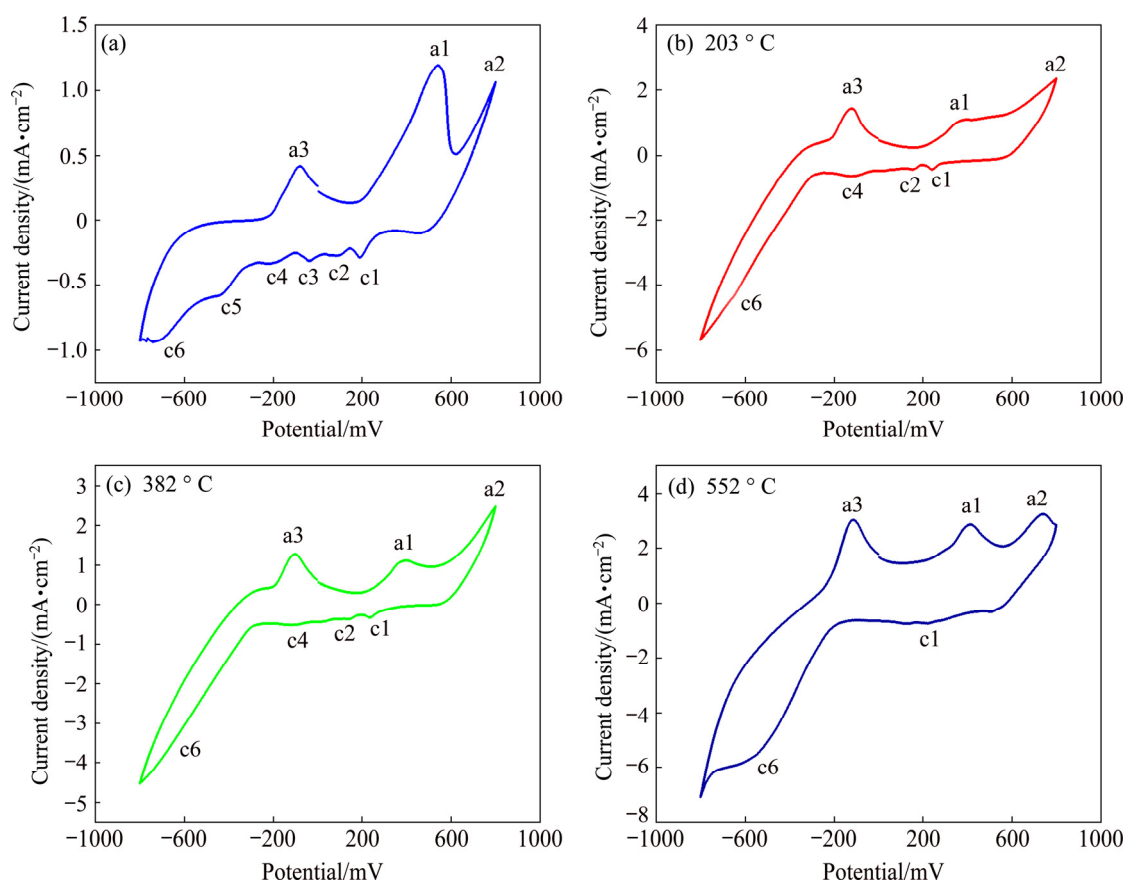
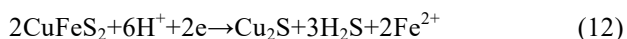
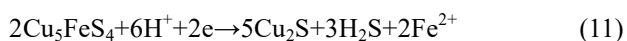


Fig. 4 Cyclic voltammograms of chalcopyrite YS (a) and three heated chalcopyrite a (b), b (c) and c (d)

chalcopyrite to chalcocite (Cu<sub>2</sub>S), as presented in Eqs. (11) and (12). When negatively scanning at the potential value of Peak c6, chalcopyrite and chalcocite were both reduced to metallic copper, as shown in Eqs. (13) and (14):



When the potential returned back to positive scan, anodic Peak a3 was proposed as the production of S<sup>0</sup> and the dissolution of Cu<sup>2+</sup> from chalcocite according to reactions (15) and (16):



It can be clearly found that with the increase in heating temperature, the electrochemical behavior of the quenched chalcopyrite electrodes was obviously different from that of the natural chalcopyrite, and the current density of the peaks was generally higher than that of initial chalcopyrite YS. On the curve of chalcopyrite c, peaks c4, c5, and c6 merged into a fairly wide and strong reduction peak in the potential range from -100 to

-700 mV, indicating that chalcopyrite c was more easily transformed to intermediate products. It has been reported that chalcopyrite is reduced to a series of intermediate copper sulfides, such as bornite, chalcocite and talnakhite, at low redox potential during the leaching process according to Eqs. (7)–(10), which should be the rate-limiting step of the bioleaching of chalcopyrite [25]. These intermediate species can be further dissolved rapidly during bioleaching. Therefore, a great change in the curve shape and the rapid formation of intermediate products should account for the high leaching rate of chalcopyrite c, and it is related to the transformation from  $\alpha$  phase to  $\beta$  phase of chalcopyrite c, as discussed above.

Meanwhile, a series of peaks (c1–c4) became unapparent in cyclic voltammograms of chalcopyrite a, b and c, especially chalcopyrite c, which should be properly considered a result of the higher oxidation–reduction rate of heated chalcopyrite. The shape of cyclic voltammetry curves and the position of electricity peaks of chalcopyrite a and b are similar to each other, but different from those of initial chalcopyrite YS and chalcopyrite c; it is clear that even if there is no change of phase, at the temperature of 203 or 382 °C, some uncertain properties of chalcopyrite change, which may explain the change in electrochemical quality.

The Tafel polarization curves of four chalcopyrite electrodes are described in Fig. 5. From the Tafel extrapolation of the curves, the electrochemical corrosion parameters are obtained, as listed in Table 2. It can be known that the increase in temperature leads to an increase in the corrosion current density and decline of the corrosion potential. Chalcopyrite c heated at 552 °C had a sharp decrease in corrosion potential (67 mV) compared to the other three chalcopyrite specimens. The corrosion currents of chalcopyrite YS and chalcopyrite a are only 0.461 and 0.457  $\mu\text{A}/\text{cm}^2$ , respectively. In contrast, chalcopyrite b and chalcopyrite c achieved corrosion currents of 0.837 and 2.221  $\mu\text{A}/\text{cm}^2$ , respectively. It is illustrated that the oxidation reaction rate of chalcopyrite increased sharply when being heated at 382 or 552 °C, which agreed fairly well with the result of bioleaching. The reasonable explanation of corrosion current increasing of chalcopyrite c at the temperature of 552 °C may be that  $\beta$ -phase chalcopyrite can be dissolved or decomposed more easily than  $\alpha$ -phase chalcopyrite.

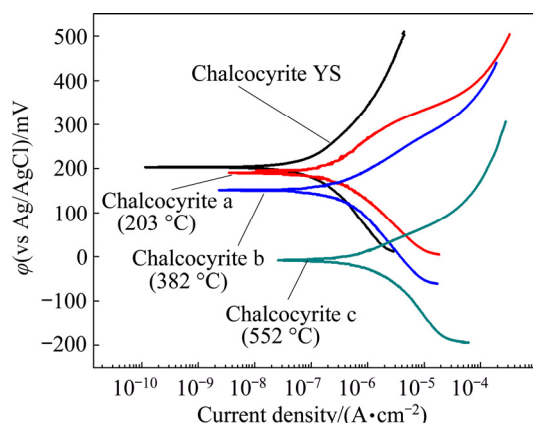


**Fig. 5** Tafel curves of chalcopyrite YS and three heated chalcopyrite electrodes

**Table 2** Corrosion parameters obtained from Tafel extrapolation of polarization curves of chalcopyrite YS and three heated chalcopyrite samples

Electrode	$b_a/$ ( $\text{mV} \cdot \text{dec}^{-1}$ )	$b_c/$ ( $\text{mV} \cdot \text{dec}^{-1}$ )	$J_{\text{corr}}/$ ( $\mu\text{A} \cdot \text{cm}^{-2}$ )	$\varphi_{\text{corr}}/$ mV
Chalcopyrite YS	174.08	166.81	0.461	207
Chalcopyrite a (203 °C)	117.59	110.88	0.457	191
Chalcopyrite b (382 °C)	88.87	148.60	0.837	174
Chalcopyrite c (552 °C)	95.59	90.51	2.221	67

### 3.4 Lattice parameters of three natural chalcopyrite samples

Table 3 gives the lattice parameters of three natural chalcopyrite samples via X-ray power diffraction. It is

apparent that different types of natural chalcopyrite with high purity have no obvious difference in lattice parameter.

**Table 3** Lattice parameters of three natural chalcopyrite samples

Chalcopyrite	$(a=b)/\text{Å}$	$c/\text{Å}$
A	$5.29012 \pm 0.000133$	$10.42017 \pm 0.000425$
B	$5.28992 \pm 0.000493$	$10.42264 \pm 0.001895$
C	$5.28913 \pm 0.000389$	$10.41770 \pm 0.001383$

### 3.5 Bioleaching of three natural chalcopyrite samples

Figure 6 shows the final copper recovery rate of three natural chalcopyrite samples in the presence of moderately thermophiles. After 19 d of bioleaching, the copper-extraction rates of chalcopyrite A, B and C were 21.4%, 25.2%, and 66.1%, respectively. Chalcopyrite C exhibited more outstanding leachability in 9K solution without ferrous ions at 45 °C than chalcopyrite A and B. By determining the lattice parameter of chalcopyrite, we found that three types of chalcopyrite had extremely close lattice parameters (Table 3). By combining the two aforementioned results, it can be inferred that it is not the unit cell size but other factors, such as impurity minerals and trace elements, which lead to different bioleaching rates of the three natural chalcopyrite samples.

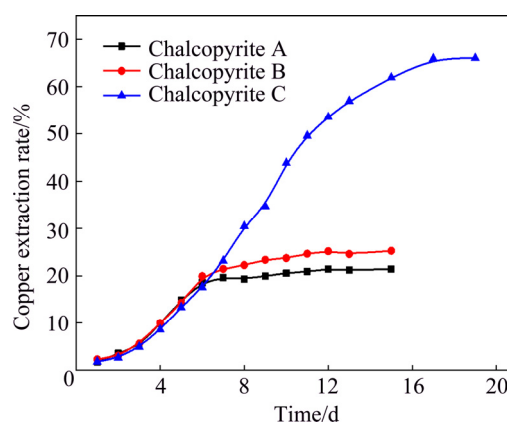
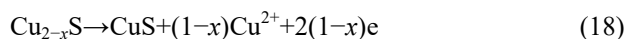


**Fig. 6** Copper extraction rates of three natural chalcopyrite samples

### 3.6 Electrochemical measurements of three natural chalcopyrite samples

Figure 7 presents the cyclic voltammograms of three different chalcopyrite electrodes in acid culture medium, starting scan from the open circuit potential of 332, 322, and 345 mV, respectively. There are six anodic oxidation peaks and four cathodic reduction peaks, of which, peaks a2, c4, c5 and c6 have been depicted in the previous section (Fig. 4). Peaks c1, c2, and c3, shown in Fig. 4, are overshadowed by each other, leading to the formation of peak c1, c2, c3, as shown in Fig. 7. In the

positive scan route, anodic peak a4 is proposed as the oxidation of metallic copper to chalcocite ( $\text{Cu}_2\text{S}$ ), as per Eq. (17). As the anodic scan continues, there are successive peaks (a5, a6, and a7) overshadowed by each other in Fig. 4 according to reactions (15) and (16) [21]. Anodic peak a8 appears, probably due to reaction (18) [22]:



As seen in Fig. 7, there is no difference in the shape of curve and the position of redox peaks among three cyclic voltammograms of natural chalcopyrite electrodes (A, B, and C). Chalcopyrite C has the higher current density of peak a2, c6, and A4 compared to chalcopyrite A and B. The higher current density of peaks (a2 and c6) in the potential of above 750 mV and below -750 mV indicates that chalcopyrite C has a higher oxidation rate at relatively high potential and a higher reduction rate at relatively low potential. The current density of anodic peak a4 of chalcopyrite C is significantly higher than that of the other two chalcopyrite electrodes, which can be explained by the rapid oxidation of metallic copper at the potential of peak c6.

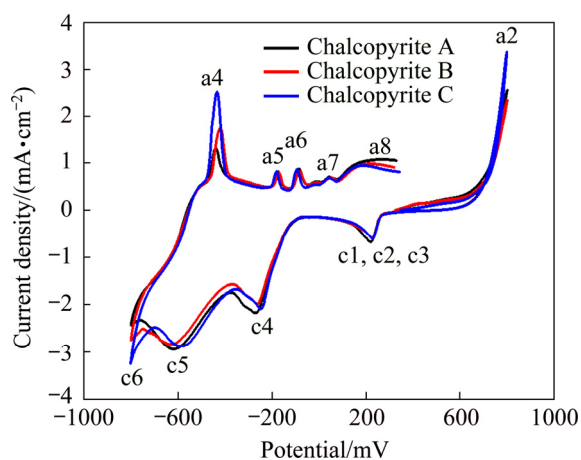


Fig. 7 Cyclic voltammograms of three natural chalcopyrite electrodes

The Tafel curves of three natural chalcopyrite samples and their corrosion parameters calculated by Tafel extrapolation are shown in Fig. 8 and Table 4, respectively. The corrosion current density of chalcopyrite C reached  $1.149 \mu\text{A}/\text{cm}^2$ , whereas that of chalcopyrite A and B was only  $0.569$  and  $0.615 \mu\text{A}/\text{cm}^2$ , respectively. Combining the result of bioleaching rate of these three chalcopyrite samples, we can infer that the higher oxidation rate accounts for the obviously high leaching rate of chalcopyrite C.

Leaching of chalcopyrite is a process of electrochemical corrosion. Different types of chalcopyrite

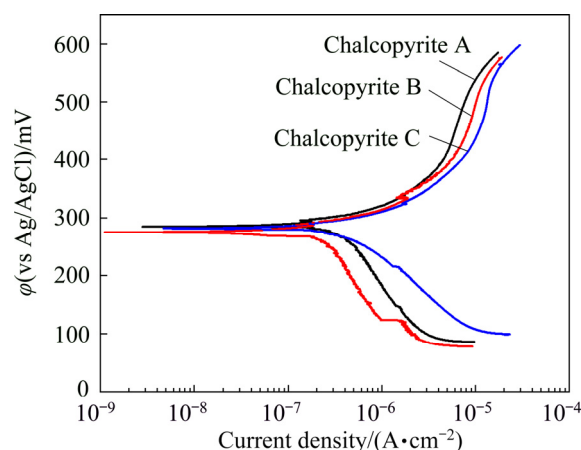


Fig. 8 Tafel curves of three natural chalcopyrite electrodes

Table 4 Corrosion parameters obtained from Tafel extrapolation of polarization curves of three natural chalcopyrite samples

Electrode	$b_a/$ ( $\text{mV} \cdot \text{dec}^{-1}$ )	$b_c/$ ( $\text{mV} \cdot \text{dec}^{-1}$ )	$J_{\text{corr}}/$ ( $\mu\text{A} \cdot \text{cm}^{-2}$ )	$\varphi_{\text{corr}}/$ mV
Chalcopyrite A	99.3	327.3	0.569	285.6
Chalcopyrite B	110.7	325.8	0.615	261.3
Chalcopyrite C	159.1	255.2	1.149	281.6

have different mineral properties and display respective electrochemical behaviors, which results in distinct bioleaching rates. It could be confirmed that other mineral properties than lattice size affect the electrochemical behavior, which results in different bioleaching behaviors of chalcopyrite.

## 4 Conclusions

(1) There was a transition from  $\alpha$  phase to  $\beta$  phase when chalcopyrite was heated at  $552 \text{ }^\circ\text{C}$  with the decrease in sulfur, and this process resulted in an increase of the lattice parameter and higher bioleaching rate. At  $382 \text{ }^\circ\text{C}$ , the dissolution of chalcopyrite could be enhanced at a low level.

(2) The bioleaching of heated chalcopyrite and three natural chalcopyrite samples indicated that the unit-cell size of chalcopyrite was unrelated to dissolution, and other mineral properties of the mineral itself affected the copper recovery.

(3) Electrochemical measurement results revealed that the chalcopyrite heated at  $552 \text{ }^\circ\text{C}$  was more easily reduced to a series of intermediate products (bornite, chalcocite and talnakhite), which could be decomposed quickly during bioleaching at a low redox potential. It could also be found that the leaching efficiency of three natural chalcopyrite samples corresponded to their corrosion rates.

## References

- [1] FERNANDO A. The use of reactors in biomining processes [J]. *Electronic Journal of Biotechnology*, 2000, 3(3): 10–11.
- [2] CÓRDOBA E M, MUÑOZ J A, BLÁZQUEZ M L, GONZÁLEZ F, BALLESTER A. Leaching of chalcopyrite with ferric ion. Part I: General aspects [J]. *Hydrometallurgy*, 2008, 93(3–4): 81–87.
- [3] LI Y, KAWASHIMA N, LI J, CHANDRA A P, GERSON A R. A review of the structure, and fundamental mechanisms and kinetics of the leaching of chalcopyrite [J]. *Advances in Colloid and Interface Science*, 2013, 197–198: 1–32.
- [4] EDELBRO R, SANDSTRÖM Å, PAUL J. Full potential calculations on the electron band structures of sphalerite, pyrite and chalcopyrite [J]. *Applied Surface Science*, 2003, 206(1–4): 300–313.
- [5] POPOV V V, KIZHAEV S A, RUD Y V. Magnetic and thermal properties of  $\text{CuFeS}_2$  at low temperatures [J]. *Physics of the Solid State*, 2011, 53(1): 71–75.
- [6] HALL S R, STEWART J M. The crystal structure refinement of chalcopyrite,  $\text{CuFeS}_2$  [J]. *Acta Crystallographica*, 1973, 29(3): 579–585.
- [7] BALÁŽ P, TKÁČOVÁ K, AVVAKUMOV E G. The effect of mechanical activation on the thermal decomposition of chalcopyrite [J]. *Journal of Thermal Analysis and Calorimetry*, 1989, 35(5): 1325–1330.
- [8] JOH V, HILLER E, PROBSTHAIN K. Thermische und röntgenographische Untersuchungen am Kupferkies [J]. *Zeitschrift Für Kristallographie*, 1956, 108(1–2): 108–129. (in German)
- [9] THIRD K A, CORD-RUWISCH R, WATLING H R. The role of iron-oxidizing bacteria in stimulation or inhibition of chalcopyrite bioleaching [J]. *Hydrometallurgy*, 2000, 57(3): 225–233.
- [10] PETERSEN J, DIXON D G. Competitive bioleaching of pyrite and chalcopyrite [J]. *Hydrometallurgy*, 2006, 83(1–4): 40–49.
- [11] MORIN D, PINCHES T, HUISMAN J, FRIAS C, NORBERG A, FORSSBERG E. Progress after three years of BioMinE—Research and technological development project for a global assessment of biohydrometallurgical processes applied to European non-ferrous metal resources [J]. *Hydrometallurgy*, 2008, 94(1): 58–68.
- [12] BALÁŽ P, KUPKA D, BASTL Z, ACHIMOVIČOVÁ M. Combined chemical and bacterial leaching of ultrafine ground chalcopyrite [J]. *Hydrometallurgy*, 1996, 42(2): 237–244.
- [13] SATO H, NAKAZAWA H, KUDO Y. Effect of silver chloride on the bioleaching of chalcopyrite concentrate [J]. *International Journal of Mineral Processing*, 2000, 59(1): 17–24.
- [14] ZHOU Shuang, GAN Min, ZHU Jian-yu, LI Qian, JIE Shi-qi, YANG Bao-jun, LIU Xue-duan. Catalytic effect of light illumination on bioleaching of chalcopyrite [J]. *Bioresource Technology*, 2015, 182: 345–352.
- [15] HIROYOSHI N, ARAI M, MIKI H, TSUNEKAWA M, HIRAJIMA T. A new reaction model for the catalytic effect of silver ions on chalcopyrite leaching in sulfuric acid solutions [J]. *Hydrometallurgy*, 2002, 63(3): 257–267.
- [16] ZHAO Hong-bo, WANG Jun, GAN Xiao-wen, ZHENG Xi-hua, TAO Lang, HU Ming-hao, LI Yi-ni, QIN Wen-qing, QIU Guan-zhou. Effects of pyrite and bornite on bioleaching of two different types of chalcopyrite in the presence of *Leptospirillum ferriphilum* [J]. *Bioresource Technology*, 2015, 194: 28–35.
- [17] DONG Ying-bo, LIN Hai, FU Kai-bin, XU Xiao-fang, ZHOU Shan-shan. Bioleaching of two different types of chalcopyrite by *Acidithiobacillus ferrooxidans* [J]. *International Journal of Minerals, Metallurgy, and Materials*, 2013, 20(2): 119–124.
- [18] MACLEAN W H, CABRI L J, GILL J E. Exsolution products in heated chalcopyrite [J]. *Canadian Journal of Earth Sciences*, 1972, 9(10): 1305–1317.
- [19] VOROB'YEV Y K, BORISOVSKIY S Y. Phase transformation and composition of chalcopyrite [J]. *International Geology Review*, 1981(9): 1023–1036.
- [20] SHIMA H. Studies on chalcopyrite (I): Transformation and dissociation of chalcopyrite heated in argon atmosphere [J]. *Journal of the Japanese Association of Mineralogists, Petrologists and Economic Geologists*, 1962, 47(4): 123–133.
- [21] GÓMEZ C, FIGUEROA M, MUÑOZ J, BLÁZQUEZ M L, BALLESTER A. Electrochemistry of chalcopyrite [J]. *Hydrometallurgy*, 1996, 43(43): 331–344.
- [22] ZENG Wei-ming, QIU Guan-zhou, ZHOU Hong-bo, CHEN Miao. Electrochemical behaviour of massive chalcopyrite electrodes bioleached by moderately thermophilic microorganisms at 48 °C [J]. *Hydrometallurgy*, 2011, 105(3–4): 259–263.
- [23] SAUBER M, DIXON D G. Electrochemical study of leached chalcopyrite using solid paraffin-based carbon paste electrodes [J]. *Hydrometallurgy*, 2011, 110(1–4): 1–12.
- [24] MUÑOZ J A, BLÁZQUEZ M L, GONZÁLEZ F, BALLESTER A, ACEVEDO F, GENTINA J C, GONZÁLEZ P. Electrochemical study of enargite bioleaching by mesophilic and thermophilic microorganisms [J]. *Hydrometallurgy*, 2006, 84(3): 175–186.
- [25] QIN Wen-qing, YANG Cong-ren, LAI Shao-shi, WANG Jun, LIU Kai, ZHANG Bo. Bioleaching of chalcopyrite by moderately thermophilic microorganisms [J]. *Bioresource Technology*, 2013, 129(Complete): 200–208.

## 温度诱导相变对黄铜矿生物浸出的影响

常可欣, 张雁生, 张家明, 李腾飞, 王军, 覃文庆

中南大学 矿物加工与生物工程学院, 长沙 410083

**摘要:** 研究黄铜矿的相变及其相态对细菌浸出的影响。在高纯氩气的保护下, 将天然黄铜矿加热到不同的温度 (203、382 和 552 °C) 以完成相变。并将黄铜矿在相变前后进行生物浸出实验。结果表明, 在 203 °C 和 382 °C 加热的黄铜矿仍处于  $\alpha$  相区, 而在 552 °C 下黄铜矿由  $\alpha$  相转变为  $\beta$  相, 3 种不同温度相变后的黄铜矿的浸出率分别为 32.9%、40.5% 和 60.95%。黄铜矿晶格增大、晶格能降低, 这是浸出率显著提高的根本原因。电化学实验表明, 随着退火温度的升高, 极化电阻降低, 腐蚀电流密度增加; 黄铜矿的氧化率越高, 浸出率就越高。

**关键词:** 晶格参数; 黄铜矿; 相变; 生物浸出; 电化学

(Edited by Bing YANG)